chemistry

MDPI

Article

Preparation of Dithiocarbamate and Carboxyl Co-Modified Chitosan and Its Adsorption of Heavy Metal Copper from Copper–Ammonia Wastewater

Chaoyang He [1], Tingting Jiang [2], Langbo Yi [1] and Wenyong Hu [1,*]

[1] School of Life Sciences, Jishou University, Jishou 416000, China
[2] College of Chemistry and Chemical Engineering, Jishou University, Jishou 416000, China
* Correspondence: huwenyong@163.com; Tel.: +86-13762157065

Abstract

To address the challenge of removing copper from copper–ammonia complex wastewater in the printed circuit board (PCB) industry, this study employed natural chitosan (CTS) as the base material. Dithiocarbamate (DTC) groups were grafted onto CTS, followed by further carboxylation (-COOH) to produce two novel adsorbents: DTC-CTS and DTC-CTS-COOH. The materials were characterized using Fourier transform infrared spectroscopy (FTIR), X-ray photoelectron spectroscopy (XPS), SEM, and related techniques. The effects of solution pH, adsorption isotherms, kinetics, and regeneration performance were systematically investigated. Characterization results confirmed the successful introduction of DTC and carboxyl (-COOH) groups. Adsorption experiments demonstrated that DTC-CTS-COOH exhibited superior Cu^{2+} adsorption performance across pH 5–8, achieving a removal efficiency of (97.67 ± 1.3)% at pH 7. Its adsorption behavior followed the Langmuir model, with a maximum adsorption capacity (Q_m) of 234.8 mg·g^{-1} at 318.15 K, significantly higher than that of DTC-CTS (183.6 mg·g^{-1}). Adsorption kinetics conformed to a pseudo-second-order model, indicating rapid adsorption rates. After five adsorption-desorption cycles, DTC-CTS-COOH maintained a Cu^{2+} removal rate above 68.41%. The synergistic interaction between -COOH and DTC functional groups enhanced the adsorbent's capacity, rate, and pH adaptability, demonstrating that DTC-CTS-COOH holds strong potential for application in the treatment of complex copper–ammonia wastewater.

Keywords: modified chitosan; dithiocarbamate; heavy metal copper; adsorption; wastewater

Check for updates

Academic Editors: Changlun Chen and Igor Alabugin

Received: 24 December 2025
Revised: 15 January 2026
Accepted: 29 January 2026
Published: 30 January 2026

Copyright: © 2026 by the authors. Licensee MDPI, Basel, Switzerland. This article is an open access article distributed under the terms and conditions of the Creative Commons Attribution (CC BY) license.

1. Introduction

With the rapid advancement of technologies such as artificial intelligence and semiconductors, printed circuit boards (PCBs), the core components of electronic devices, have found increasingly widespread applications, driving explosive growth in the global market [1,2]. However, this booming PCB manufacturing industry also poses significant environmental challenges [3]. Production processes such as alkaline etching and electroless copper plating generate large volumes of copper- and ammonia-rich wastewater [4]. Studies have shown that even after pretreatment, the concentration of ammonia nitrogen in PCB wastewater can reach approximately 200 mg·L^{-1} [5], while copper ion concentrations in certain process effluents can exceed 100,000 mg·L^{-1}, along with strong acidity [6]. If discharged without adequate treatment, such wastewater can lead to eutrophication of water bodies and heavy metal accumulation in soils [7,8]. Moreover, through bioaccumulation in the food chain, it may pose serious health risks to humans, including liver

damage and neurotoxicity [9,10]. The coexistence of high ammonia nitrogen, high copper content, and acidity creates a complex pollution profile, making efficient copper removal from PCB wastewater a major technical bottleneck in achieving the industry's sustainable and green development.

Current mainstream technologies for treating copper-containing wastewater include chemical precipitation [11,12], sulfidation [13], electrolysis [14], and adsorption [15,16]. However, methods such as chemical precipitation and electrolysis often exhibit low removal efficiency and high energy consumption when applied to low-concentration copper wastewater [17]. Sulfidation, typically implemented via Na_2S dosing, not only poses the risk of toxic H_2S emission, particularly in acidic or pH-fluctuating wastewater streams common in industrial scenarios, but also requires cumbersome pre-neutralization steps that elevate operational costs and complexity [18]. Among these technologies, adsorption stands out for its ability to selectively remove target ions through both physical interactions (e.g., van der Waals forces, pore retention) and chemical interactions (e.g., coordination chelation, ion exchange) between the adsorbent and heavy metal ions [19]. Owing to its low cost, operational simplicity, and strong adaptability without the need for complex equipment, adsorption has emerged as one of the most promising approaches for the treatment of copper-containing wastewater [20,21].

Chitosan (CTS), a natural cationic polysaccharide derived from seafood processing by-products such as shrimp and crab shells, is renewable, biodegradable, and environmentally friendly [22]. Owing to the abundance of amino (-NH_2) and hydroxyl (-OH) groups along its molecular chain, which exhibit a strong affinity toward heavy metal ions. As a result, chitosan has attracted widespread attention in the treatment of heavy metal-containing wastewater [23]. However, in treating PCB wastewater characterized by complex composition and variable acidity, single DTC modification still requires further optimization. The chelation efficiency of DTC groups can be compromised under highly acidic conditions (pH < 4) due to protonation of the nitrogen sites, which reduces their electron-donating ability and coordination strength. Moreover, in the presence of high concentrations of competing ammonia, the formation of stable copper–ammonia complexes ($[Cu(NH_3)_4]^{2+}$) further challenges the selectivity and removal efficiency of DTC-modified adsorbents [24,25].

Dithiocarbamate (DTC) represents a class of typical heavy metal chelating agents. The sulfur (S) and nitrogen (N) atoms within their molecular structure can act as coordination centers, forming stable and insoluble chelates with heavy metal ions such as Cu^{2+}, thereby exhibiting excellent selectivity and adsorption performance [26,27]. Grafting DTC functional groups onto the CTS backbone is an effective approach to overcome the inherent limitations of chitosan. Studies have shown that DTC modification not only significantly enhances the capacity of chitosan to sequester heavy metals but also broadens the applicable pH range of the material and accelerates the adsorption kinetics [28]. However, in treating PCB wastewater characterized by complex composition and variable acidity, single DTC modification still requires further optimization.

To address this, this study employs a dual-modification strategy by incorporating dithiocarbamate (DTC) and carboxyl (-COOH) groups into CTS. The DTC groups can form stable, insoluble chelates with Cu^{2+}, thereby significantly enhancing the coordinative adsorption capacity for heavy metal ions [29]. Meanwhile, the introduction of -COOH groups not only strengthens Cu^{2+} capture through electrostatic interactions but also extends the material's applicability over a broader pH range [30,31]. The synergistic interaction between DTC and -COOH functionalities is expected to markedly enhance the overall adsorption performance and environmental adaptability of CTS-based adsorbents.

Therefore, this study aims to address the following scientific question: How does the synergistic interaction between DTC and -COOH groups enhance the adsorption capacity and pH adaptability of chitosan-based adsorbents in copper–ammonia complex wastewater? To answer this, we propose and test the following specific hypotheses: (1) The coexistence of DTC and -COOH on CTS will synergistically enhance the adsorption capacity and rate for Cu^{2+} in ammonia-rich wastewater through combined coordination and electrostatic interactions. (2) The introduction of -COOH groups will improve the surface hydrophilicity and charge-tuning ability of the material, thereby extending its effective pH range to acidic and neutral conditions. (3) The adsorption process will be dominated by chemisorption, and its mechanism can be elucidated through systematic characterization of functional groups along with kinetic and thermodynamic analysis. This work is expected to provide an efficient and adaptable adsorbent design strategy for the treatment of copper–ammonia wastewater from PCB manufacturing.

2. Materials and Methods

2.1. Raw Materials

All reagents used in this study were of analytical grade. CTS (degree of deacetylation $\geq$ 95%), carbon disulfide (CS_2, 99.0%), isopropanol (C_3H_8O, 99.5%), and chloroacetic acid ($C_2H_3ClO_2$, 99.5%) were obtained from Shanghai McLean Biochemical Technology Co., Ltd., Shanghai, China. Sodium hydroxide (NaOH, 96.0%), hydrochloric acid (HCl, 38%), anhydrous ethanol (C_2H_6O, 99.7%), copper sulfate pentahydrate ($CuSO_4 \cdot 5H_2O$, 99.0%), and ammonium chloride (NH_4Cl, 99.5%) were purchased from Chengdu Jinshan Chemical Reagent Co., Ltd., Chengdu, China. Deionized water was used throughout all experiments.

2.2. Preparation of Adsorbent

2.2.1. Synthesis of DTC-CTS

To synthesize DTC-CTS, 2.0 g of CTS was accurately weighed and transferred into a 250 mL three-necked flask. Subsequently, 50 mL of C_3H_8O was added as a dispersion medium, and the mixture was magnetically stirred for 30 min to ensure uniform dispersion. Then, 10 mL of a 5% (*w*/*v*) NaOH aqueous solution was slowly added along the inner wall of the flask under continuous stirring at room temperature for 1 h to activate the $-NH_2$ groups on the CTS molecular chains. The CTS to CS_2 molar ratio of 1:3 was selected based on preliminary experiments and previous reports [32] to maximize DTC grafting yield while minimizing reagent excess. CS_2 was then added dropwise at a rate of one drop every 2 s, with a molar ratio of CTS to CS_2 of 1:3. After addition, the reaction temperature was raised to 30 °C and maintained under constant magnetic stirring for 4 h. Upon completion, the pH of the system was adjusted to 7.0 using 1% HCl and 1% NaOH solutions. The resulting precipitate was collected by centrifugation (8000 r·min^{-1}, 10 min) and washed three times with 50% ethanol, followed by C_2H_5OH to remove unreacted CS_2 and impurities. The final product was dried to constant weight in a vacuum oven at 50 °C to obtain DTC-CTS. The synthesis route is illustrated in Figure 1.

2.2.2. Preparation of DTC-CTS-COOH

(1) Preparation of CTS-COOH

To synthesize CTS-COOH, 5.0 g of CTS was accurately weighed and transferred into a 500 mL three-necked flask. Then, 100 mL of C_3H_8O was added, and the mixture was magnetically stirred for 30 min to achieve complete dispersion. Subsequently, 20 mL of a 5% (*w*/*v*) NaOH aqueous solution was added dropwise under continuous stirring at 25 °C for 1 h to activate the $-NH_2$ and -OH groups on the CTS chains. $C_2H_3ClO_2$ (2.4 g), weighed according to a 1:4 molar ratio of CTS to $C_2H_3ClO_2$, was dissolved in 10 mL of C_3H_8O with

ultrasonication and then slowly added to the flask. After complete addition, the reaction temperature was increased to 50 °C and maintained under constant magnetic stirring for 3 h to complete the carboxylation process. The resulting mixture was neutralized to pH 7.0 with 1 mol·L^{-1} HCl, and the precipitate was collected by centrifugation (8000 r·min^{-1}, 10 min). The product was washed three times with 50% ethanol, followed by C_2H_5OH, and then dried in a vacuum oven at 50 °C to constant weight to obtain CTS-COOH.

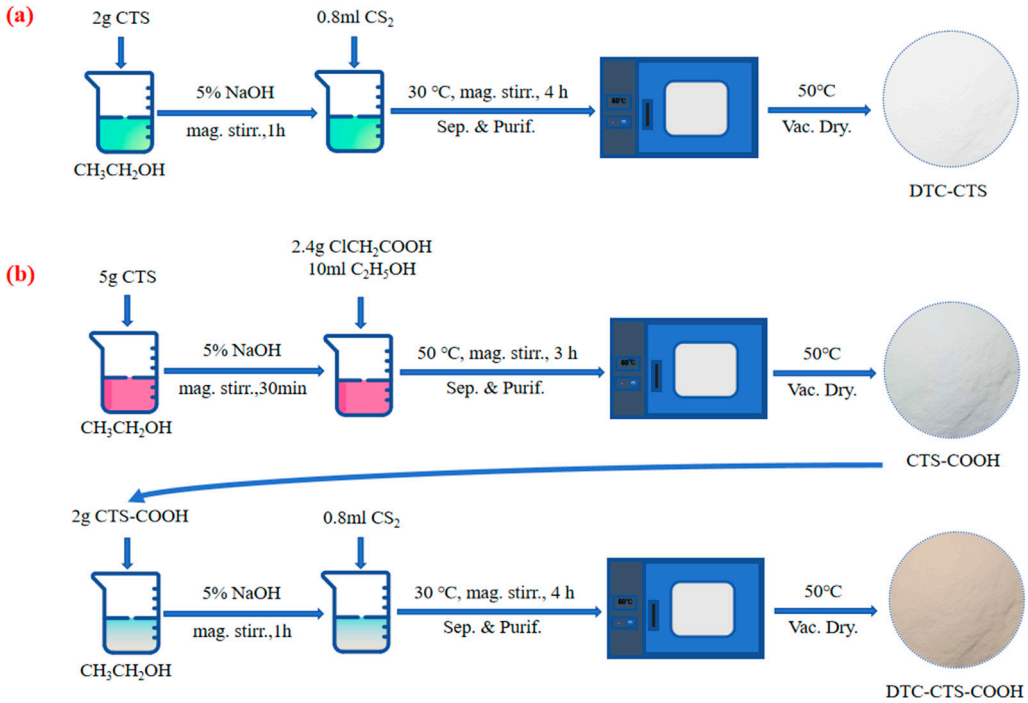


Figure 1. Schematic diagram of adsorbent synthesis: (**a**) DTC-CTS; (**b**) DTC-CTS-COOH.

(2) Preparation of DTC-CTS-COOH

To synthesize DTC-CTS-COOH, 2.0 g of CTS-COOH was accurately weighed and placed into a 250 mL three-necked flask. Then, 50 mL of C_3H_8O and 10 mL of a 5% (*w*/*v*) NaOH aqueous solution were added. The mixture was magnetically stirred at room temperature for 1 h to activate the reactive sites. Subsequently, 0.8 mL of CS_2 was added dropwise at a controlled rate, maintaining a molar ratio of CTS-COOH to CS_2 of 1:3. After complete addition, the reaction was continued under magnetic stirring at 30 °C for 4 h to facilitate the grafting of DTC groups. Upon completion, the pH of the reaction mixture was adjusted to 5–6 using a 1% HCl solution. The precipitate was collected by centrifugation (8000 r·min^{-1}, 10 min) and washed three times with 50% ethanol, followed by C_2H_5OH to remove unreacted reagents and impurities. Finally, the product was dried in a vacuum oven at 50 °C to constant weight, yielding the DTC- and -COOH-co-modified CTS (DTC-CTS-COOH). The synthesis route is illustrated in Figure 1.

2.3. Sample Characterization

The samples were characterized using Fourier transform infrared spectroscopy (FTIR, Thermo Fisher Scientific Nicolet IS20, Waltham, MA, USA) within the wavenumber range of 500–4000 cm^{-1}. The spectra of the powdered samples were obtained using the potassium bromide (KBr, purity ≥ 99.0%, Tianjin Guangfu Technology Development Co., Ltd., Tianjin, China) pellet method. The surface morphology of the adsorbents was examined using scanning electron microscopy (SEM, Zeiss Sigma 300, Oberkochen, Germany). Furthermore, the elemental composition and chemical states of C, O, and S were analyzed

using X-ray photoelectron spectroscopy (XPS, Thermo Scientific K-Alpha, Waltham, MA, USA) to confirm the successful introduction of functional groups. The bulk elemental composition of the samples was determined using an elemental analyzer (Elementar Vario EL, Langenselbold, Germany).

2.4. Batch Adsorption Experiments

2.4.1. pH Effect Experiment

Simulated wastewater, prepared to mimic the characteristics of PCB production effluent, was formulated using $CuSO_4 \cdot 5H_2O$ and NH_4Cl. The initial concentrations of Cu^{2+} and ammonia nitrogen were both adjusted to 200 mg·L^{-1}. Before use, the solution was filtered through a 0.45 μm aqueous membrane filter to remove suspended impurities and stored for subsequent experiments.

A 100 mL aliquot of simulated copper–ammonia wastewater (initial Cu^{2+} concentration: 200 mg·L^{-1}) was transferred into a conical flask. The solution pH was adjusted to values between 1 and 8 using 1 mol·L^{-1} HCl or NaOH. The pH range of 1–8 was chosen to avoid Cu^{2+} precipitation above pH 8 and to cover the typical acidic to weakly alkaline conditions of PCB wastewater. Since copper precipitation becomes significant at pH > 8, the range of 1–8 was selected to simulate the weakly alkaline to acidic conditions typical of PCB wastewater. All experiments were performed in triplicate. Accurately weighed 100 mg portions of DTC-CTS and DTC-CTS-COOH adsorbents were added to the flasks, which were then placed in a constant-temperature shaker (25 °C, 200 r·min^{-1}) for 2 h. After adsorption, 5 mL of the suspension was sampled, centrifuged at 4000 r·min^{-1} for 10 min, and the supernatant was filtered through a 0.45 μm membrane. The residual Cu^{2+} concentration in the filtrate was determined using inductively coupled plasma optical emission spectrometry (ICP-OES, PerkinElmer Avio 200, Waltham, MA, USA).

Calculation method: The total copper removal rate R is calculated using Equation (1):

$$R = \frac{C_0 - C_e}{C_0} \times 100\% \quad (1)$$

where C_0 is the initial total copper concentration in the wastewater (mg·L^{-1}), and C_e is the total copper concentration at adsorption equilibrium (mg·L^{-1}).

2.4.2. Adsorption Isotherm

Accurately weighed 100 mg of DTC-CTS adsorbent was added to 100 mL of Cu^{2+} simulated solutions with initial concentrations of 50, 100, 150, 200, 300, and 500 mg·L^{-1}. The solution pH was adjusted to 5.0, and adsorption experiments were conducted at three temperatures: 298.15, 308.15, and 318.15 K. The mixtures were placed in a thermostatic water-bath shaker and agitated at 120 r·min^{-1} until adsorption equilibrium was achieved. After equilibrium, the suspensions were centrifuged, and the supernatants were filtered through 0.45 μm membrane filters. The residual Cu^{2+} concentrations were determined using ICP-OES (PerkinElmer Avio 200, Waltham, MA, USA). The same experimental procedure was applied to the DTC-CTS-COOH adsorbent.

Linear fitting analyses were conducted based on the Langmuir (Equation (2)) and the Freundlich (Equation (3)) adsorption isotherm models.

$$\frac{C_e}{Q_e} = \frac{C_e}{Q_m} + \frac{1}{K_L Q_m} \quad (2)$$

$$\ln Q_e = \frac{1}{n} \ln C_e + \ln K_F \quad (3)$$

where Q_e and Q_m represent the equilibrium adsorption capacity and theoretical maximum adsorption capacity, respectively, $mg \cdot g^{-1}$; K_L is the Langmuir adsorption constant, $L \cdot mg^{-1}$; 1/n is the heterogeneity factor; and K_F is the Freundlich adsorption constant $[(mg \cdot g^{-1}) \cdot (L \cdot mg^{-1})^{1/n}]$.

2.4.3. Adsorption Kinetics

Simulated Cu^{2+} solutions with initial concentrations of 100 and 200 $mg \cdot L^{-1}$ were prepared and adjusted to pH 5.0. A total of 100 mg of DTC-CTS adsorbent was accurately weighed and added to 100 mL of each solution. The mixtures were placed in a thermostatic water bath shaker and agitated at 25 °C and 120 $r \cdot min^{-1}$. At predetermined time intervals (1–480 min), three parallel 5 mL samples were withdrawn, filtered through a 0.45 μm membrane filter, and analyzed for Cu^{2+} concentration using ICP-OES. The same procedure was applied to the DTC-CTS-COOH adsorbent.

The experimental data were fitted using the pseudo-first-order (Equation (4)) and pseudo-second-order (Equation (5)) kinetic models to elucidate the adsorption kinetics and underlying rate-controlling mechanisms.

$$\ln (Q_e - Q_t) = \ln Q_e - K_1 t \quad (4)$$

$$\frac{t}{Q_t} = \frac{1}{K_2 Q_e^2} + \frac{t}{Q_e} \quad (5)$$

where Q_t is the amount of Cu^{2+} adsorbed at time t, $mg \cdot g^{-1}$; K_1 is the pseudo-first-order kinetic rate constant, min^{-1}; K_2 is the pseudo-second-order kinetic rate constant, $g \cdot (mg \cdot min)^{-1}$.

2.5. Adsorption Cycling Experiment

At pH 5.0 and 25 °C, 100 mg of DTC-CTS-COOH was added to 100 mL of a 200 $mg \cdot L^{-1}$ Cu^{2+} solution and shaken for 2 h. After solid–liquid separation, desorption was performed at 25 °C for 12 h using HCl, NaOH, and EDTA-2Na as eluents. The adsorbent was then washed with ultrapure water, dried, and reused in the subsequent adsorption cycle. This adsorption–desorption process was repeated five times to evaluate the reusability of the adsorbent.

3. Results and Discussion

3.1. Adsorption Agent Characterization

3.1.1. FTIR Analysis

The FTIR spectra of CTS and DTC-CTS-COOH are presented in Figure 2. As previously reported [33], the main characteristic peaks of CTS are observed at 3442.3 cm^{-1} (O-H and N-H stretching vibrations), 2874.4 cm^{-1} (C-H stretching in methylene groups), 1627.1 cm^{-1} and 1603.3 cm^{-1} (C=O stretching in residual acetamide groups), and 1154 cm^{-1} and 1025.4 cm^{-1} (C-O-C stretching vibrations). Compared with CTS, the FTIR spectrum of DTC-CTS exhibits new characteristic peaks at 1486.1 cm^{-1} (-NCSS group) and 949.3 cm^{-1}, confirming the successful introduction of the DTC group.

Meanwhile, the disappearance of the C=O stretching bands at 1627.1 cm^{-1} and 1603.3 cm^{-1}, along with the emergence of a new absorption peak near 1603.3 cm^{-1}, indicates that -COOH groups existed in the form of carboxylate salts. This is likely due to the alkaline synthesis conditions and the washing process with only distilled water and ethanol [34]. These spectral changes collectively verify the successful synthesis of the DTC-CTS-COOH material.

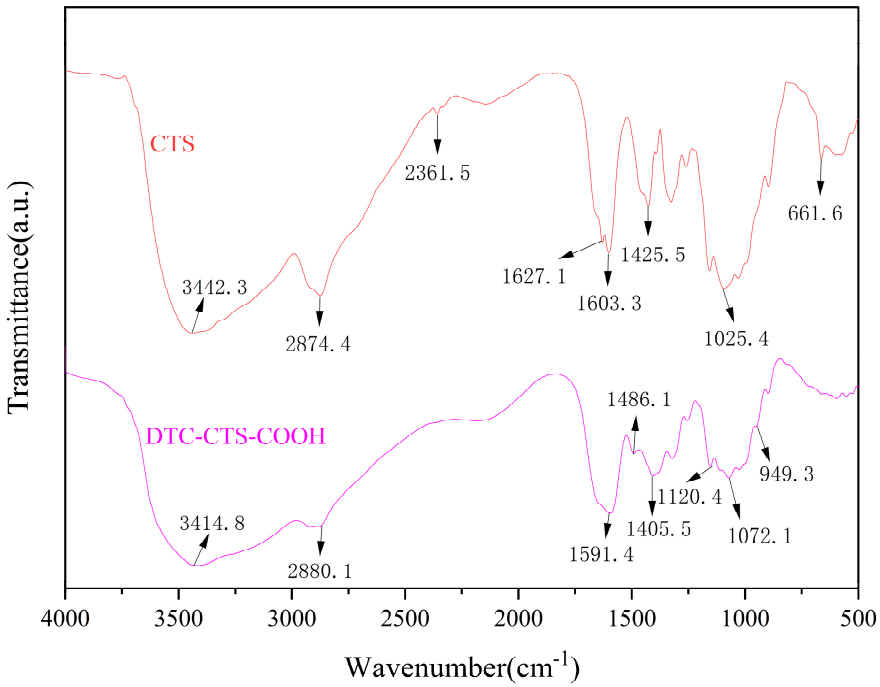


Figure 2. FTIR spectra of CTS and DTC-CTS-COOH.

3.1.2. SEM Analysis

The morphological evolution of the materials before and after modification was directly visualized using scanning electron microscopy (SEM), as presented in Figure 3. The pristine chitosan exhibits a characteristically smooth, dense, and relatively featureless surface Figure 3a, which inherently limits the accessibility of its native functional groups (-NH_2, -OH) and results in a low specific surface area. This compact microstructure is a key morphological factor contributing to its limited adsorption capacity. Upon grafting with DTC groups, a remarkable transformation is observed, as shown in Figure 3b. The surface of DTC-CTS becomes distinctly roughened and fragmented, showing a loosely aggregated, granular morphology with visible cracks and wrinkles. This textural development is attributed to the alkaline reaction conditions and the introduction of bulky DTC moieties, which disrupt the original hydrogen-bonding network within the chitosan matrix, thereby creating more exposed surfaces and potential pores.

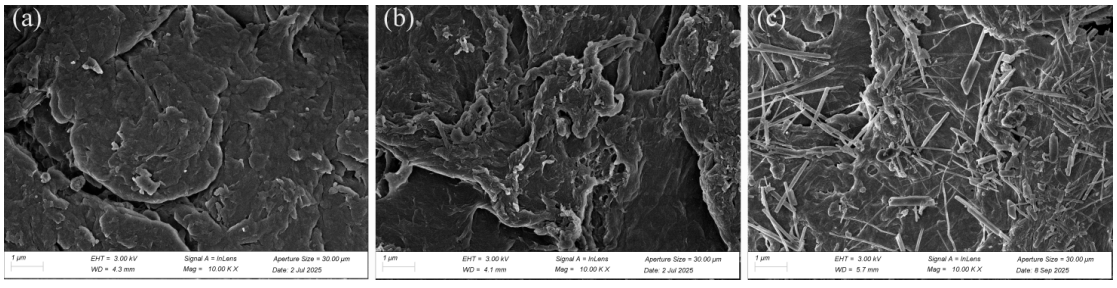


Figure 3. SEM images of (**a**) CTS; (**b**) DTC-CTS; (**c**) DTC-CTS-COOH.

The most significant microstructural advancement is achieved with the dual-functionalized adsorbent, DTC-CTS-COOH (Figure 3c). Its surface transitions into a highly developed, porous, and coral-like architecture. This intricate three-dimensional network, featuring interconnected pores and vastly increased surface roughness, is the synergistic outcome of sequential carboxylation and dithiocarbamation. These consecutive reactions profoundly etch and reconstruct the polymer backbone. Crucially, this optimized morphol-

ogy is not merely a visual change but a structural enhancement with direct implications for adsorption performance. The dramatically increased surface area and porous framework facilitate superior mass transfer of copper and copper–ammonia complex ions from the bulk solution to the adsorbent surface. More importantly, this open and accessible microstructure ensures maximum exposure of the grafted DTC and -COOH functional groups, allowing for their synergistic chelation and electrostatic interactions with Cu^{2+} to proceed with high efficiency. Therefore, the progressive microstructural evolution from a smooth film to a porous network provides compelling physical evidence for successful chemical modification and establishes a clear structure–property relationship, explaining the enhanced adsorption capacity and kinetics of DTC-CTS-COOH at a microscopic level.

3.1.3. XPS Analysis

The XPS spectra of DTC-CTS and DTC-CTS-COOH are presented in Figure 4. Deconvolution of the C 1s spectra for both samples reveals characteristic peaks corresponding to C-N (283.3 eV), C-C (284.8 eV), and C-O (286.2 eV) bonds. Notably, DTC-CTS-COOH exhibits an additional peak at 287.5 eV, assigned to the O-C=O group, confirming the successful introduction of -COOH functionalities [35,36]. Similarly, deconvolution of the O 1s spectra shows peaks at 529.7 eV (O-H) and 531.3 eV (C-O-C) in both samples. In contrast, DTC-CTS-COOH displays a distinct $-COO^-$ peak at 534.1 eV, further validating the incorporation of -COOH groups [36,37]. In addition, the S 2p spectra for both modified CTSs exhibit two characteristic peaks at 160.0 eV (C-S $2p_{3/2}$) and 161.2 eV (C-S 2p $n_{1/2}$), corresponding to thioester (S=C-S) structures. These results collectively confirm the successful introduction of both sulfur- and -COOH-containing functional groups into the CTS matrix [38].

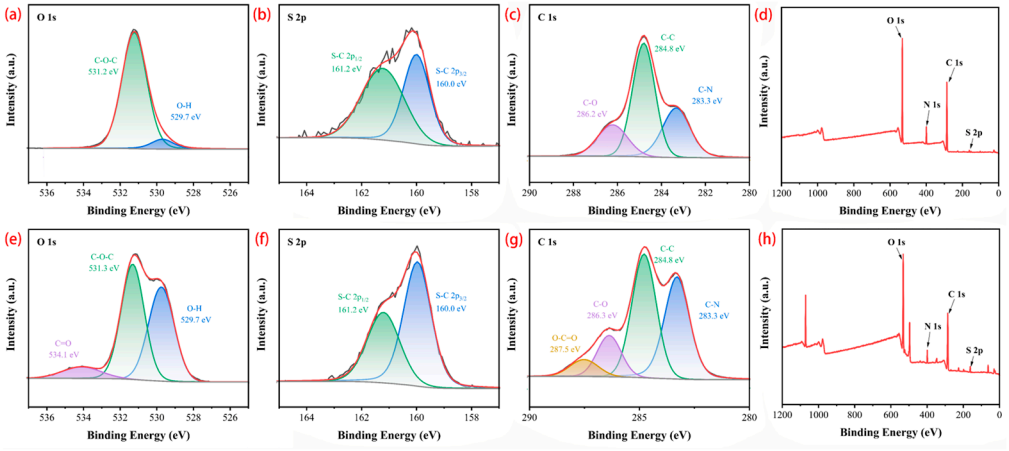


Figure 4. XPS spectra of DTC-CTS and DTC-CTS-COOH: (**a**,**e**) O 1s, (**b**,**f**) S 2p, (**c**,**g**) C 1s, and (**d**,**h**) survey spectra.

3.1.4. Elemental Analysis

Elemental analysis was conducted on the raw material, intermediates, and final products to quantitatively evaluate the reaction progress. The results for CTS, DTC-CTS, and DTC-CTS-COOH are summarized in Table 1. Compared with CTS, DTC-CTS shows a sulfur mass fraction of 3.1%, confirming the successful incorporation of DTC groups onto the CTS backbone. Moreover, the C/N molar ratio of DTC-CTS-COOH is higher than that of CTS, despite the absence of any additional nitrogen sources during the synthesis. This suggests that an extra carbon source was introduced during the modification process, likely derived from $C_2H_3ClO_2$ or CS_2.

Table 1. Elemental analysis before and after adsorption.

Material Name	Element Content (%)				
	C	H	N	S	Cu
CTS	43.8	6.5	8.2	0	-
DTC-CTS	47.5	6.2	6.5	3.1	-
DTC-CTS-COOH	49.2	7.8	5.9	2.0	-
DTC-CTS (after)	41.2	5.8	5.9	2.8	12.4
DTC-CTS-COOH (after)	42.1	6.5	5.2	1.7	18.6

Additionally, for the post-Cu^{2+}-adsorption samples in Table 1, namely DTC-CTS (after) and DTC-CTS-COOH (after), the presence of Cu (with mass fractions of 12.4% and 18.6%, respectively) directly confirms the effective Cu^{2+} uptake by the materials. Meanwhile, the slight decreases in S and N contents, which are key components of DTC groups, as exemplified by the drop in S content of DTC-CTS from 3.1% to 2.8%, also support the mechanism that S and N participate in the coordination chelation of Cu^{2+}.

3.2. Adsorption Study

3.2.1. Effect of Initial Wastewater pH

Figure 5 illustrates the variation in copper removal efficiency from copper–ammonia wastewater by the two adsorbents as a function of pH after 2 h of adsorption. The adsorption performance of both materials is clearly affected by the solution pH, exhibiting a trend of initial increase followed by a gradual decrease. Notably, DTC-CTS-COOH demonstrates a significantly broader effective pH range compared to DTC-CTS.

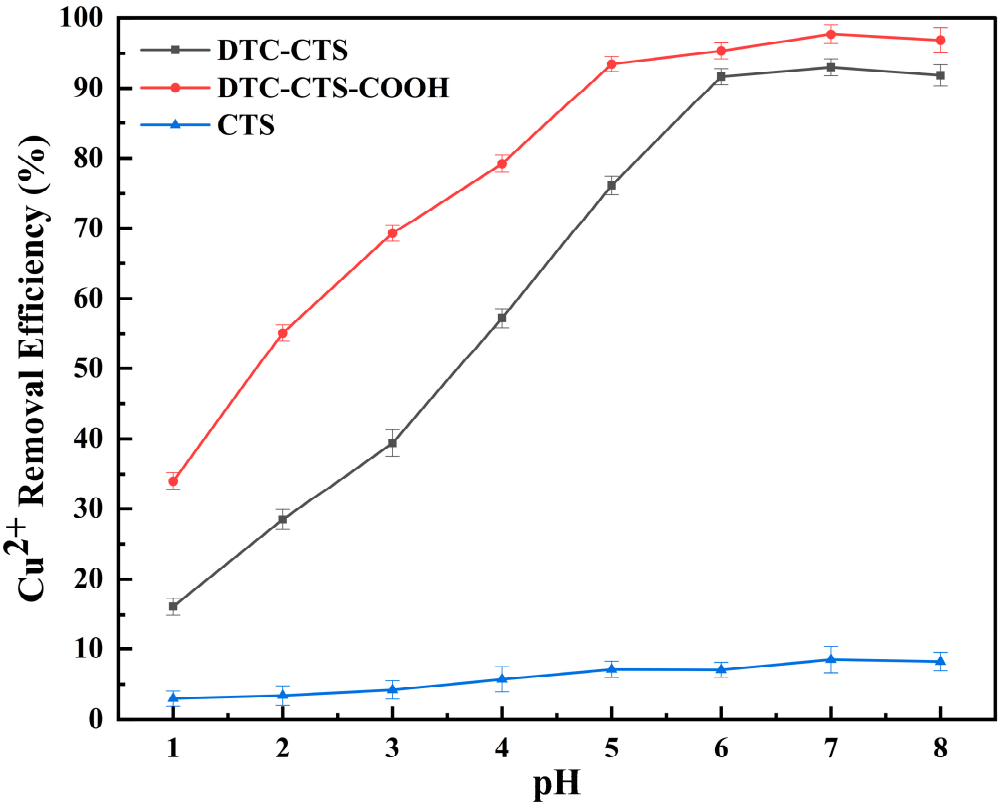


Figure 5. Effect of pH on the adsorption of Cu^{2+}.

For DTC-CTS, the adsorption behavior is mainly governed by the coordination ability of the DTC groups. Under acidic conditions (pH < 5), the high concentration of H^+ ions

protonates the active sites, thereby reducing their chelating capability [39]. In addition, the strongly acidic environment hampers competition with the stable copper–ammonia complexes ($[Cu(NH_3)_4]^{2+}$), further weakening adsorption. As the pH increases toward neutrality (pH 6–8), the DTC groups become fully ionized and can effectively coordinate with the complexed copper ions, achieving a maximum removal efficiency of 93.01% near pH 7. However, under more alkaline conditions, the increased stability of copper–ammonia complexes suppresses adsorption, leading to a slight decline in removal efficiency [40].

In contrast, DTC-CTS-COOH exhibits superior and broader pH adaptability, maintaining effective adsorption performance even under mildly acidic conditions (optimal range expanded to pH $\geq$ 5) and achieving a maximum copper removal efficiency of 97.67 $\pm$ 1.3% at pH 7. This enhancement is attributed to the introduction of -COOH groups, which not only improve the pH tolerance of the adsorbent but also generate a synergistic adsorption effect with the DTC groups. Overall, these results demonstrate that DTC-CTS-COOH possesses an excellent potential for the efficient treatment of copper–ammonia wastewater, particularly from PCB manufacturing sources.

3.2.2. Adsorption Isotherms

The results of the adsorption isotherm model fitting are presented in Table 2 and Figure 6. The Langmuir model exhibited high linear correlation coefficients at all tested temperatures, and the calculated maximum adsorption capacities closely matched the experimental values. This consistency indicates that the Langmuir model accurately describes the adsorption behavior of the modified CTS toward Cu^{2+}, suggesting that the process is primarily dominated by monolayer adsorption. In the Freundlich model, the 1/n value reflects adsorption intensity; across all temperatures, 1/n values were below 0.014, signifying a strong affinity of the adsorbents for Cu^{2+} and favorable adsorption conditions.

Table 2. Fitting parameters of adsorption isotherms for DTC-CTS and DTC-CTS-COOH.

Adsorbent	Temperature (K)	Langmuir Isotherm Parameters			Freundlich Isotherm Parameters		
		Q_m (mg·g^{-1})	K_L (L·mg^{-1})	r_L	K_F [(mg·g^{-1})·(L·mg^{-1})$^{1/n}$]	n	r_F
DTC-CTS	298.15	162.2	0.21	0.9891	71.25	0.15	0.7808
	308.15	174.0	0.22	0.9939	73.02	0.165	0.8380
	318.15	183.6	0.24	0.9927	75.52	0.17	0.8618
DTC-CTS-COOH	298.15	209.8	2.54	0.9959	93.4	0.16	0.8421
	308.15	223.4	2.35	0.9879	97.97	0.17	0.8742
	318.15	234.8	2.21	0.9811	101.91	0.17	0.8933

Note: r_F is the correlation coefficient for the Freundlich isotherm adsorption model fitting equation.

A comparison of the two modified CTS adsorbents revealed that DTC-CTS-COOH exhibited markedly superior adsorption capacity and binding strength. Its Langmuir maximum adsorption capacity (Q_m = 209.8–234.8 mg·g^{-1}) was over 30% higher than that of DTC-CTS (Q_m = 162.2–183.6 mg·g^{-1}). Compared to adsorbents reported in the literature, DTC-CTS-COOH exhibits significant performance advantages. For instance, its maximum adsorption capacity (234.8 mg·g^{-1}) is notably higher than that of dual-DTC-modified chitosan (194 mg·g^{-1}) [32] and diethylenetriamine-grafted chitosan (147 mg·g^{-1}) [41], demonstrating a superior capability for Cu^{2+} uptake. This improvement can be attributed to the synergistic interaction between the electrostatic enrichment provided by the -COOH groups and the strong coordination capability of the DTC groups, which collectively enhance the capture efficiency of copper–ammonia complex ions. Furthermore, the Langmuir adsorption constant (K_L = 2.11–2.54 L·mg^{-1}) of DTC-CTS-COOH was significantly higher than that of DTC-CTS (K_L = 0.21–0.24 L·mg^{-1}), confirming that the incorporation

of -COOH groups promotes ion enrichment near active sites, reduces diffusion resistance, and improves the initial adsorption rate [42].

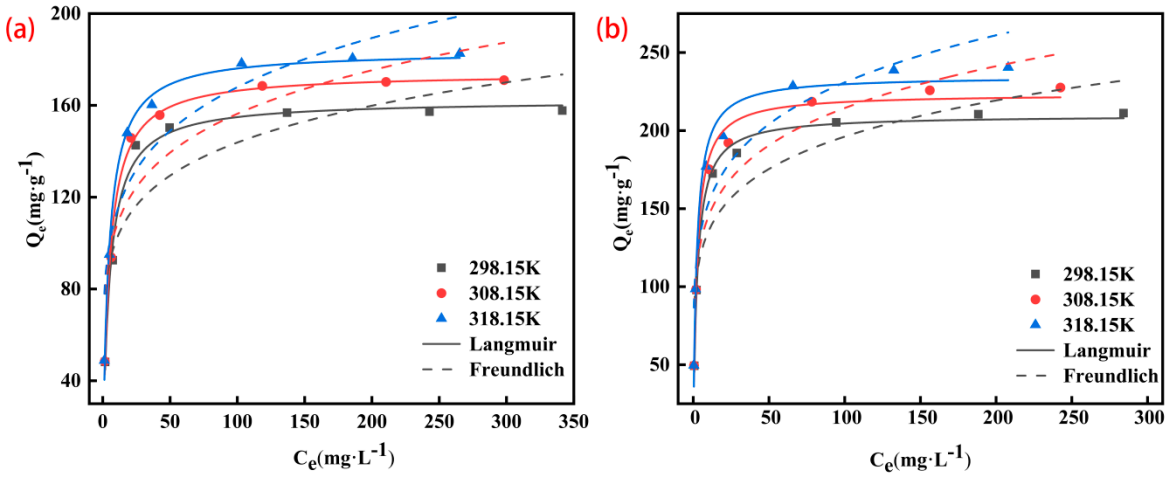


Figure 6. Fitting of adsorption isotherm models for Cu(II) on two modified adsorbents: (**a**) DTC-CTS, (**b**) DTC-CTS-COOH.

Temperature also had a positive effect on adsorption performance. Within the range of 298.15–318.15 K, the Q_m values of DTC-CTS and DTC-CTS-COOH increased by 13.2% and 11.9%, respectively. As shown in Figure 6, the adsorption capacity gradually increased with rising temperature, indicating that higher temperatures favor the adsorption process. This phenomenon may be attributed, based on the properties of copper–ammonia complexes, to the thermal dissociation of the complexes and the enhancement of their coordination with the active sites on the adsorbent surface.

3.2.3. Adsorption Kinetics

The adsorption capacity of the modified CTS toward Cu^{2+} increased rapidly during the initial adsorption stage (0–40 min), followed by a gradual deceleration, and ultimately reached equilibrium at approximately 120 min. The adsorption behavior of Cu^{2+} on the modified CTS was analyzed using the pseudo-first-order (Equation (4)) and pseudo-second-order (Equation (5)) kinetic models, with the fitting results summarized in Table 3.

Table 3. Kinetic fitting parameters of DTC-CTS and DTC-CTS-COOH.

Name		**DTC-CTS**		**DTC-CTS-COOH**	
Adsorption Kinetic Model	**Cu^{2+} Initial Concentration (mg·L^{-1})**	**100**	**200**	**100**	**200**
Pseudo-first-order kinetics	k_1 (min^{-1})	0.036	0.038	0.94	0.93
	Q_e (mg·g^{-1})	77.68	132.14	82.89	154.89
	R^2	0.9682	0.9515	0.9818	0.9766
Pseudo-second-order kinetics	k_2 (g·mg^{-1}·min^{-1})	0.42	0.27	0.79	182.45
	Q_e (mg·g^{-1})	94.13	158.43	98.05	0.47
	R^2	0.9822	0.9723	0.9909	0.9932

As illustrated in Figure 7, the adsorption amount (Q_t) exhibited a characteristic rapid increase before reaching equilibrium. The kinetic fitting results reveal that the adsorption of Cu^{2+} by both adsorbents conforms well to the pseudo-second-order model, as evidenced by the higher determination coefficients (R^2 = 0.9723–0.9932) compared with those of the pseudo-first-order model (R^2 = 0.9515–0.9818). This indicates that the adsorption process is primarily governed by chemisorption, involving sulfur-nitrogen coordination

through the DTC groups and electrostatic synergism from the -COOH groups. At higher initial Cu^{2+} concentrations (200 mg·L^{-1}), the kinetic advantage of DTC-CTS-COOH becomes more pronounced. The electrostatic enrichment capability of the -COOH groups enhances Cu^{2+} concentration near the adsorbent surface, reducing diffusion resistance and accelerating coordination interactions. In contrast, DTC-CTS, which relies mainly on coordination adsorption, is more strongly affected by mass transfer limitations. In summary, the incorporation of -COOH groups into the DTC-modified CTS significantly improves adsorption kinetics through an electrostatic acceleration-coordination capture mechanism, enabling DTC-CTS-COOH to achieve rapid and efficient Cu^{2+} removal within a short contact time [43,44].

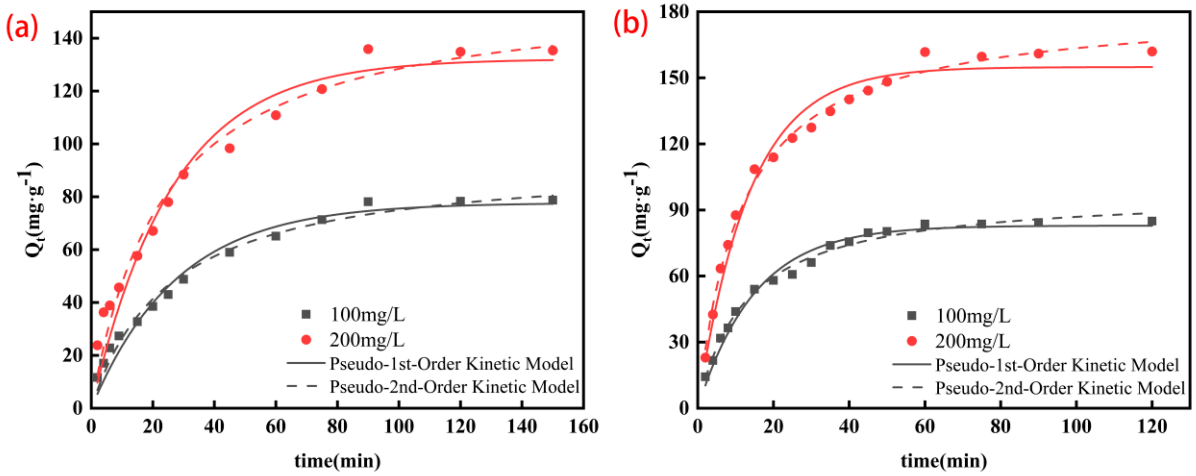


Figure 7. Kinetic model fitting for Cu^{2+} adsorption onto (**a**) DTC-CTS and (**b**) DTC-CTS-COOH.

3.3. Regeneration and Stability of Adsorbents

From a practical application perspective, in addition to adsorption capacity, the regenerability and stability of the adsorbent are equally crucial. After five consecutive adsorption-desorption cycles, the Cu^{2+} removal efficiencies of DTC-CTS-COOH were 94.57%, 87.34%, 75.13%, 71.05%, and 68.41%, respectively. The gradual decline in removal efficiency with increasing cycles can be attributed to the partial and irreversible loss of active sites during regeneration. The complexation and electrostatic interactions involved in Cu^{2+} adsorption may induce conformational changes in functional groups or reduce their chemical activity. Moreover, repeated chemical elution can lead to minor structural degradation or pore collapse in the adsorbent matrix, further decreasing the number of available adsorption sites. Despite these effects, DTC-CTS-COOH maintained a Cu^{2+} removal rate above 68.41% after five cycles, demonstrating favorable reusability and structural stability. These results suggest that DTC-CTS-COOH possesses strong potential for sustainable application in the cyclic treatment of copper–ammonia wastewater.

3.4. Discussion on Adsorption Mechanisms and Synergistic Effects

Based on comprehensive characterization and adsorption behavior analysis, this study proposes that the adsorption of Cu^{2+} by DTC-CTS-COOH is driven by the synergistic effects of the following multiple mechanisms, which are key to the material's high performance.

Coordination chelation serves as the core mechanism. The successfully grafted DTC groups are rich in sulfur (S) and nitrogen (N) electron-donating atoms, which can form stable five-membered chelate structures with Cu^{2+}. This chelation is characterized by high strength and selectivity; even in the presence of coexisting ammonia nitrogen, the affinity of DTC for Cu^{2+} is significantly greater than its coordination with NH_3. This enables effective

competition for and capture of the $[Cu(NH_3)_4]^{2+}$ complexes in wastewater, as directly evidenced by the chemical shift observed in the S 2p XPS spectra after adsorption.

The mechanism of electrostatic attraction and pH buffering is of critical importance. The introduced -COOH groups dissociate into $-COO^-$ under near-neutral to weakly alkaline conditions (pH > pKa), imparting a negative charge to the material surface. This creates a strong Coulombic attraction for the positively charged copper–ammonia complex ions. This not only directly contributes to the adsorption capacity but, more importantly, helps maintain the surface negativity across a broader pH range (especially pH 5–7), thereby expanding the effective working window. This explains the superior pH adaptability of DTC-CTS-COOH compared to DTC-CTS.

A notable pre-concentration and synergistic enhancement effect exists. The -COOH groups pre-concentrate Cu^{2+} ions and their complexes near the adsorbent surface through electrostatic interactions, effectively increasing the local metal ion concentration around the active sites and reducing mass transfer diffusion resistance. This significantly promotes the subsequent efficient coordination reaction between these ions and the DTC groups. This tandem mechanism of "electrostatic enrichment followed by enhanced chelation" results in a synergistic "1 + 1 > 2" effect due to the coexistence of DTC and -COOH groups.

While coordination and electrostatic attraction are the primary proposed mechanisms, alternative pathways such as ion exchange or surface-induced precipitation at higher pH could contribute marginally to Cu^{2+} uptake. However, the excellent fit to the Langmuir model and the pseudo-second-order kinetics (chemisorption) strongly support that the specific chemical interactions with DTC and -COOH groups are dominant under the studied conditions [45,46].

Together, these mechanisms contribute to the comprehensive enhancement in the adsorption capacity (Q_m), adsorption rate (k_2), and pH applicability observed for DTC-CTS-COOH. Therefore, the adsorption process is not governed by a single physical or chemical interaction but is a composite mechanism dominated by chemical coordination, significantly assisted and facilitated by electrostatic attraction, with both aspects working in a synergistic and reinforcing manner. The specific adsorption mechanism is illustrated in Figure 8.

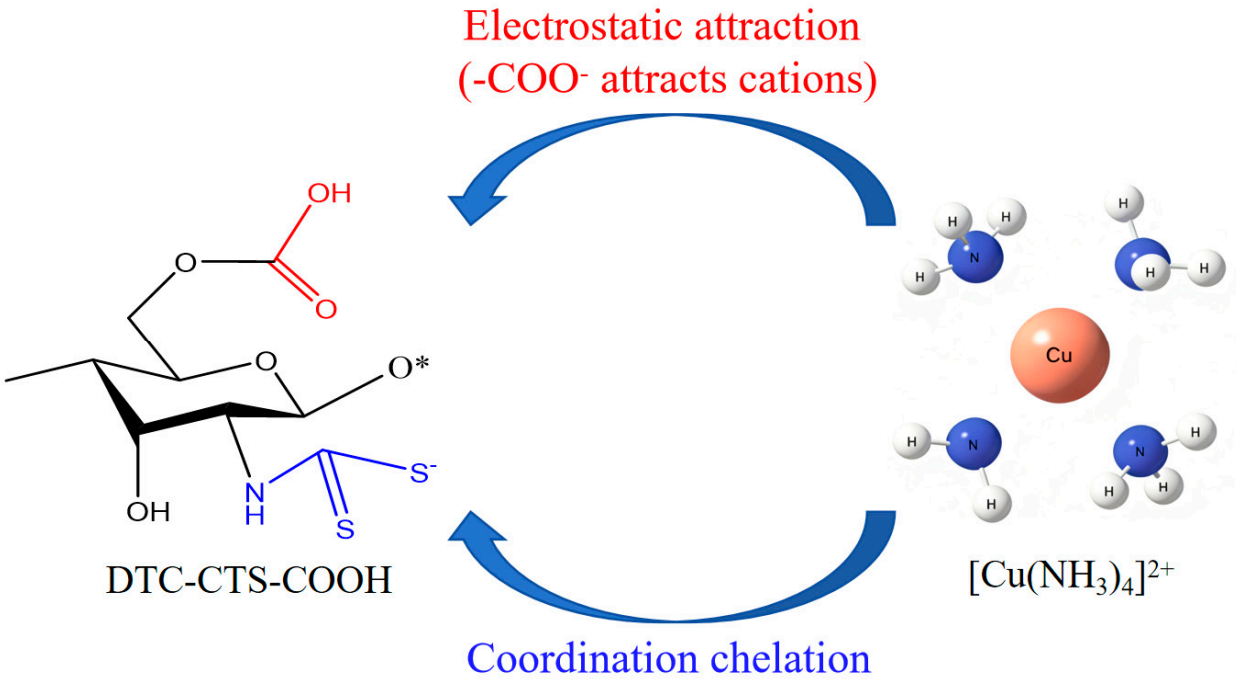


Figure 8. Schematic illustration of the adsorption mechanism of DTC-CTS-COOH.

3.5. Limitations and Generalizability of Findings

This study calibrated key adsorption parameters, namely initial Cu^{2+}/ammonia nitrogen concentrations and pH levels from 1 to 8, to match the typical characteristics of PCB effluent, ensuring direct relevance to the target application. Yet, the validity of these findings in real-world scenarios is constrained by inherent limitations that merit attention.

Notably, the competitive effects of coexisting contaminants in actual PCB wastewater remain unaddressed. Real industrial effluents often contain additional heavy metals (e.g., Pb^{2+}, Cd^{2+}) and organic ligands (e.g., EDTA, citrate), which could either compete with Cu^{2+} for the DTC and -COOH active sites on the adsorbent or form more stable Cu^{2+} complexes. This means the reported $97.67 \pm 1.3\%$ Cu^{2+} removal efficiency is only verified under single-component conditions; how DTC-CTS-COOH performs in multi-pollutant matrices still needs systematic confirmation.

Equally critical is the mismatch between experimental design and industrial practice. All tests were conducted in controlled batch mode, characterized by constant temperature, fixed agitation, and the use of pre-filtered simulated wastewater. In contrast, real-world applications rely primarily on continuous-flow systems such as fixed-bed or fluidized-bed reactors. Factors that profoundly influence treatment efficacy, including flow rate, adsorbent packing density, and mass transfer efficiency, were not considered. Moreover, real wastewater often contains suspended solids or colloids that can cause adsorbent fouling over time and compromise long-term stability, a factor not accounted for in our short-term batch experiments.

The study also lacks the broad generalizability of the findings beyond PCB copper–ammonia wastewater. We focused exclusively on this specific system; the adsorbent's performance for free Cu^{2+} in non-ammoniacal solutions, or for heavy metals with distinct ionic radii and coordination preferences (e.g., Hg^{2+}, Cr^{6+}), remains uncharacterized. The synergistic mechanism between DTC and -COOH groups, tailored to Cu^{2+} coordination and electrostatic interactions, cannot be assumed to translate to other contaminants.

The practical industrial adoption of this method faces further uncertainties, as regeneration was evaluated over only five cycles. Therefore, the long-term structural stability, including potential degradation of DTC functional groups or leaching of sulfur and nitrogen species during repeated elution cycles, remains unverified. Additionally, we did not assess the cost-effectiveness of large-scale synthesis (e.g., reagent consumption of CS_2 and chloroacetic acid) or the feasibility of eluent recovery, both of which are pivotal for real-world deployment. Environmental variables like fluctuating ionic strength (from PCB etching processes) and extreme temperature variations, which could alter adsorbent–solution interactions, were also not explored.

In summary, DTC-CTS-COOH shows significant potential for efficient Cu^{2+} removal from typical PCB copper–ammonia wastewater under controlled laboratory conditions. However, its efficacy in complex real matrices, continuous-flow systems, and for other heavy metals remains unproven. Future research should prioritize multi-pollutant competitive systems, long-term stability in real wastewater, scale-up performance in continuous reactors, and a comprehensive cost–benefit analysis to bridge the gap between laboratory promise and industrial applicability.

4. Conclusions

This study aimed to address the challenge of removing copper from complex ammonia-rich wastewater by developing a dual-functionalized chitosan-based adsorbent. Guided by the hypotheses that DTC and -COOH groups would synergistically enhance adsorption capacity, extend the effective pH range, and be governed by a chemisorption-dominated mechanism, a novel adsorbent, DTC-CTS-COOH, was successfully synthesized and evalu-

ated alongside its single-functionalized counterpart, DTC-CTS. The optimized adsorbent achieved a maximum copper removal efficiency of (97.67 ± 1.3)%, and its adsorption behavior followed the Langmuir model, with a maximum adsorption capacity (Q_m) of 234.8 $mg \cdot g^{-1}$ at 318.15 K, significantly higher than that of DTC-CTS (183.6 $mg \cdot g^{-1}$).

The key findings confirm that the strategic dual-modification imparted superior performance. DTC-CTS-COOH demonstrated a significantly broader operational pH window (pH 5–8) and a higher maximum adsorption capacity compared to DTC-CTS, attributable to the synergistic interplay between the strong coordination of DTC groups and the electrostatic enrichment/buffering effect of -COOH groups. The adsorption process was best described by the Langmuir isotherm and the pseudo-second-order kinetic model, underscoring a monolayer, chemisorption-dominated mechanism. Furthermore, DTC-CTS-COOH exhibited promising regenerability, retaining over two-thirds of its initial efficiency after five cycles, highlighting its potential for sustainable applications.

This work demonstrates a viable strategy for enhancing the performance of biopolymer-based adsorbents in complex wastewater through targeted multi-functionalization, contributing to the rational design of efficient and adaptable materials for heavy metal removal. On a practical level, the dual-functionalized adsorbent offers a potentially safer and more operationally simple alternative to conventional treatments such as sulfide precipitation, particularly for the challenging acidic-to-neutral copper-ammonia wastewater commonly generated in the PCB industry.

While the present study provides a systematic performance evaluation under well-controlled conditions, certain aspects warrant further exploration. Post-adsorption characterization (e.g., SEM, XPS) could be extended, and additional analyses—such as porosity (BET), selectivity in the presence of co-existing ions, and advanced techniques like AFM or XRF—would help to refine the mechanistic understanding and complete the material profile. Future research could therefore focus on (1) validating the adsorbent's performance in real industrial wastewater containing multiple competing ions; (2) conducting fixed-bed column tests to assess its scalability and dynamic behavior in continuous-flow systems; and (3) carrying out a thorough life-cycle and techno-economic analysis to evaluate its practical feasibility for industrial implementation.

In summary, this research successfully demonstrates the efficacy of a DTC/COOH co-modification strategy in creating an adaptable and efficient chitosan-based adsorbent, presenting a significant step forward in developing advanced materials for the targeted treatment of heavy metals in complex aquatic environments.

Author Contributions: C.H.: Conceptualization, Methodology, Formal analysis, Writing—Original Draft, Validation; T.J.: Visualization, Writing—Review and Editing; L.Y.: Resources; W.H.: Writing—Review and Editing. All authors have read and agreed to the published version of the manuscript.

Funding: This research was partially supported by the Natural Science Foundation of Hunan Province [grant number 2024JJ7403].

Data Availability Statement: The data that support the findings of this study are available from the corresponding author upon reasonable request.

Conflicts of Interest: The authors declare no conflicts of interest.

References

1. Baldini, E.; Chessa, S.; Brogi, A. Estimating the environmental impact of green IoT deployments. *Sensors* **2023**, *23*, 1537. [CrossRef] [PubMed]
2. Chang, Y.; Deng, L.; Meng, X.; Zhang, W.; Wang, C.; Wang, Y.; Zhao, S.; Lin, L.; Crittenden, J.C. Closed-loop electrochemical recycling of spent copper (II) from etchant wastewater using a carbon nanotube modified graphite felt anode. *Environ. Sci. Technol.* **2018**, *52*, 5940–5948. [CrossRef] [PubMed]

3. Sundeep, D.; Varadharaj, E.K.; Sastry, C.C. Fabrication of industrial grade F/g-C_3N_4 reinforced banana natural Fiber sustainable PCB substrates. *Sci. Rep.* **2025**, *15*, 19894. [CrossRef] [PubMed]
4. Cong, P.; Zhang, Y.; Zhang, J.; Mohammad, A. Two-sectional struvite formation process for enhanced treatment of copper–ammonia complex wastewater. *Trans. Nonferrous Met. Soc. China* **2017**, *27*, 457–466.
5. Xu, J.-J.; Jin, J.-A.; Yu, Y.; Lu, H.-F.; Jin, R.-C. Feasibility of anaerobic ammonium oxidation process for treatment of pretreated printed circuit board wastewater. *Bioresour. Technol.* **2023**, *388*, 129766. [CrossRef]
6. Guo, Y.; Zheng, J.; Yan, X.; Liu, X.; Xu, W.; Liu, W.; Li, X.; Lin, Z. Recovery of copper from printed circuit board (PCB) acidic etching wastewater: Ammonia regulates the crystallization of high valued copper salt. *Surf. Interfaces* **2022**, *31*, 101969. [CrossRef]
7. Liu, Q.; Zhou, T.; Liu, Y.; Wu, W.; Wang, Y.; Liu, G.; Wei, N.; Yin, G.; Guo, J. Typical Heterotrophic and Autotrophic Nitrogen Removal Process Coupled with Membrane Bioreactor: Comparison of Fouling Behavior and Characterization. *Membranes* **2024**, *14*, 214. [CrossRef]
8. Li, L.; Gao, K.; Yang, M.; Zheng, Q.; Zhang, M.; Deng, X. Challenges and potential solutions of microalgae-based systems for wastewater treatment and resource recovery. *Front. Bioeng. Biotechnol.* **2023**, *11*, 1210228. [CrossRef]
9. Pankit, A.N.; Bhave, S.A. Copper metabolic defects and liver disease: Environmental aspects. *J. Gastroenterol. Hepatol.* **2002**, *17*, S403–S407. [CrossRef]
10. Gaetke, L.M.; Chow-Johnson, H.S.; Chow, C.K. Copper: Toxicological relevance and mechanisms. *Arch. Toxicol.* **2014**, *88*, 1929–1938. [CrossRef]
11. Li, Y.; Lin, G.; Hongping, C.; Jun, L.; Zhenwei, L. Removing Copper from Electroplating Wastewater by Chemical Precipitation. *Environ. Sci. Technol.* **2011**, *34*, 149–151. [CrossRef]
12. Wang, Q.; Yu, J.; Chen, X.; Du, D.; Wu, R.; Qu, G.; Guo, X.; Jia, H.; Wang, T. Non-thermal plasma oxidation of Cu (II)-EDTA and simultaneous Cu (II) elimination by chemical precipitation. *J. Environ. Manag.* **2019**, *248*, 109237. [CrossRef]
13. Jiang, S.; Fu, F.; Qu, J.; Xiong, Y. A simple method for removing chelated copper from wastewaters: Ca (OH) 2-based replacement-precipitation. *Chemosphere* **2008**, *73*, 785–790. [CrossRef]
14. Qian, A.; Liao, P.; Yuan, S.; Luo, M. Efficient reduction of Cr (VI) in groundwater by a hybrid electro-Pd process. *Water Res.* **2014**, *48*, 326–334. [CrossRef]
15. Koppula, S.; Jagasia, P.; Panchangam, M.K.; Surya, S.B.M. Synthesis of bimetallic Metal-Organic Frameworks composite for the removal of Copper (II), Chromium (VI), and Uranium (VI) from the aqueous solution using fixed-bed column adsorption. *J. Solid State Chem.* **2022**, *312*, 123168. [CrossRef]
16. Cui, L.; Wang, Y.; Gao, L.; Hu, L.; Yan, L.; Wei, Q.; Du, B. EDTA functionalized magnetic graphene oxide for removal of Pb (II), Hg (II) and Cu (II) in water treatment: Adsorption mechanism and separation property. *Chem. Eng. J.* **2015**, *281*, 1–10. [CrossRef]
17. Guillem-Navajas, A.; Martín-Illán, J.Á.; Salagre, E.; Michel, E.G.; Rodriguez-San-Miguel, D.; Zamora, F. Iron oxyhydroxide-covalent organic framework nanocomposite for efficient as (III) removal in water. *ACS Appl. Mater. Interfaces* **2022**, *14*, 50163–50170. [CrossRef] [PubMed]
18. Peng, C.; Chai, L.; Tang, C.; Min, X.; Song, Y.; Duan, C.; Yu, C. Study on the mechanism of copper–ammonia complex decomposition in struvite formation process and enhanced ammonia and copper removal. *Acad. J. Environ. Sci.* **2017**, *51*, 222–233. [CrossRef]
19. Fu, F.; Wang, Q. Removal of heavy metal ions from wastewaters: A review. *J. Environ. Manag.* **2011**, *92*, 407–418. [CrossRef]
20. Yi, L.; Shuqin, Z.; Dajun, R.; Xiaoqing, Z. Research Progress on Adsorption of Heavy Metals by Modified Chitosan with Different Functional Groups. *Chem. Reag.* **2022**, *44*, 495–503.
21. Li, Q.; Lai, S.; Yang, Y. Experimental Study on Cu2+Removal by DTC-Type Heavy Metal Capture Agents. *J. Zhejiang Univ. (Nat. Sci. Ed.)* **2014**, *41*, 78–81.
22. Zhang, W.; An, Y.; Li, S.; Liu, Z.; Chen, Z.; Ren, Y.; Wang, S.; Zhang, X.; Wang, X. Enhanced heavy metal removal from an aqueous environment using an eco-friendly and sustainable adsorbent. *Sci. Rep.* **2020**, *10*, 16453. [CrossRef] [PubMed]
23. Aranaz, I.; Alcántara, A.R.; Civera, M.C.; Arias, C.; Elorza, B.; Heras Caballero, A.; Acosta, N. Chitosan: An overview of its properties and applications. *Polymers* **2021**, *13*, 3256. [CrossRef] [PubMed]
24. Zhang, Y.; Luo, X. Preparation of chitosan/sodium polystyrene sulfonate composite microsphere and its adsorption performance for copper(II) in wastewater. *Metall. Anal.* **2025**, *45*, 76–83. [CrossRef]
25. Kumar, M.R.; Muzzarelli, R.A.; Muzzarelli, C.; Sashiwa, H.; Domb, A. Chitosan chemistry and pharmaceutical perspectives. *Chem. Rev.* **2004**, *104*, 6017–6084. [CrossRef]
26. Morita, F.; Nakakubo, K.; Yunoshita, K.; Endo, M.; Biswas, F.B.; Nishimura, T.; Mashio, A.S.; Hasegawa, H.; Taniguchi, T.; Maeda, K. Dithiocarbamate-modified cellulose-based sorbents with high storage stability for selective removal of arsenite and hazardous heavy metals. *RSC Adv.* **2020**, *10*, 30238–30244. [CrossRef]
27. Wang, X.; Qi, F.; Xiong, J.; Zhao, J.; Zhang, G.; Afzal, S.; Gu, X.; Li, Q.; Luo, S.; Mo, H. Synthesis of a novel dithiocarbamate surfactant derivative adsorbent for efficient removal of heavy metal ions. *ACS Omega* **2023**, *8*, 41512–41522. [CrossRef]

28. Xu, H.; Tang, R.; Cao, Z.; Luo, H.; Shen, Y. Adsorption Properties of Chitosan X an thogenate for Copper(II). *Chin. J. Appl. Chem.* **2008**, *25*, 673–676.
29. Yang, W.; Li, J.; Li, Y.; Zhao, H. Thioharnish-modified GO material and its adsorption performance for Cu2+. *J. Jilin Univ. (Sci. Ed.)* **2024**, *62*, 444–451. [CrossRef]
30. Zhang, D.; Zhou, W.; Wei, B.; Wang, X.; Tang, R.; Nie, J.; Wang, J. Carboxyl-modified poly (vinyl alcohol)-crosslinked chitosan hydrogel films for potential wound dressing. *Carbohydr. Polym.* **2015**, *125*, 189–199. [CrossRef]
31. Miao, L.; Deng, W.; Chen, X.; Gao, M.; Chen, W.; Ao, T. Selective adsorption of phosphate by carboxyl-modified activated carbon electrodes for capacitive deionization. *Water Sci. Technol.* **2021**, *84*, 1757–1773. [CrossRef]
32. Cao, Y.; He, W.; Xiang, B.; Li, Y. Synthesis and Properties of DI-DTC-Modified Chitosan. *Technol. Water Treat.* **2008**, *34*, 35–38.
33. Yin, Z.; Qiu, D.; Zhang, M. Molecular level study of cadmium adsorption on dithiocarbamate modified chitosan. *Environ. Pollut.* **2021**, *271*, 116322. [CrossRef] [PubMed]
34. Zhang, Q.I.; Zhang, W.; Sun, S.; Dong, Z.; Zhang, J. Comprehensive adsorption experiment of carboxylated graphene oxide for Cu(II). *Exp. Technol. Manag.* **2019**, *36*, 66–70. [CrossRef]
35. Pei, S.; Liu, F.; Li, Z.; Ma, L.; Abdiryim, T.; Xu, F.; You, J.; Tan, Y.; Liu, X. Bimetallic cobalt-iron metal organic framework loaded chitosan cryogel for rapid activation of peroxymonosulfate to degrade tetracycline. *J. Colloid Interface Sci.* **2025**, *703*, 139059. [CrossRef]
36. Lee, D.U.; Kayumov, M.; Park, J.; Park, S.K.; Kang, Y.; Ahn, Y.; Kim, W.; Yoo, S.H.; Park, J.-K.; Kim, B.-G. Antibiofilm and antithrombotic hydrogel coating based on superhydrophilic zwitterionic carboxymethyl chitosan for blood-contacting devices. *Bioact. Mater.* **2024**, *34*, 112–124. [CrossRef] [PubMed]
37. Wang, S.; Cai, J.; Shi, J.; Shao, X.; Cai, L.; Hou, L. In situ synthesis of Chitin/ZIF-67 composite hydrogel for efficient recovery of high purity acetonitrile by removal of Zn^{2+} and Ag^{+}. *Chem. Eng. J.* **2024**, *499*, 156457. [CrossRef]
38. Pang, K.; Sun, W.; Ye, F.; Yang, L.; Pu, M.; Yang, C.; Zhang, Q.; Niu, J. Sulfur-modified chitosan derived N, S-co-doped carbon as a bifunctional material for adsorption and catalytic degradation sulfamethoxazole by persulfate. *J. Hazard. Mater.* **2022**, *424*, 127270. [CrossRef]
39. Wu, T.; Wang, Z.; Lu, Y.; Liu, S.; Li, H.; Ye, G.; Chen, J. Graphene oxide membranes for tunable ion sieving in acidic radioactive waste. *Adv. Sci.* **2021**, *8*, 2002717. [CrossRef]
40. Durán, S.V.; Lapo, B.; Meneses, M.; Sastre, A.M. Recovery of neodymium (III) from aqueous phase by chitosan-manganese-ferrite magnetic beads. *Nanomaterials* **2020**, *10*, 1204. [CrossRef]
41. Yi, Y.; Wang, Y. Synthesis and Characterization of Diethylene Triamine Derivative of Chitosan. *Ion Exch. Adsorpt.* **2006**, *22*, 33–38.
42. Jasem-Feisal, A.; Amiripour, F.; Ghasemi, S. MOF-derived Co-Al layered double hydroxide modified rice husk biochar nanohybrid for efficient removal of Cu (II) from wastewater. *J. Water Process. Eng.* **2024**, *64*, 105612. [CrossRef]
43. Simonin, J.-P. On the comparison of pseudo-first order and pseudo-second order rate laws in the modeling of adsorption kinetics. *Chem. Eng. J.* **2016**, *300*, 254–263. [CrossRef]
44. Ezzati, R.; Azizi, M.; Ezzati, S. A theoretical approach for evaluating the contributions of pseudo-first-order and pseudo-second-order kinetics models in the Langmuir rate equation. *Vacuum* **2024**, *222*, 113018. [CrossRef]
45. Zhang, Z.; Lai, J.; Yin, H.; Feng, X.; Tan, W.; Liu, F. Absorption mechanisms of Cu^{2+} on a biogenic bixbyite-like Mn_2O_3 produced by Bacillus CUA isolated from soil. *Geochem. Trans.* **2015**, *16*, 5. [CrossRef]
46. Alghamdi, A.G.; Alasmary, Z. Efficient remediation of cadmium-and lead-contaminated water by using Fe-modified date palm waste biochar-based adsorbents. *Int. J. Env. Res. Public Health* **2023**, *20*, 802. [CrossRef]

Disclaimer/Publisher's Note: The statements, opinions and data contained in all publications are solely those of the individual author(s) and contributor(s) and not of MDPI and/or the editor(s). MDPI and/or the editor(s) disclaim responsibility for any injury to people or property resulting from any ideas, methods, instructions or products referred to in the content.